Status of the PIENU experiment at TRIUMF

2015 J. Phys.: Conf. Ser. 631 012044

(http://iopscience.iop.org/1742-6596/631/1/012044)

Journal of Physics: Conference Series **631** (2015) 012044 doi:10.1088/1742-6596/631/1/012044

Status of the PIENU experiment at TRIUMF

S.Ito[1], A.Aguilar-Arevalo[2], M.Aoki[1], M.Blecher[3], D.I.Britton[4], D.A. Bryman[5], D. vom Bruch[5], S.Chen[6], J.Comfort[7], S.Cuen-Rochin[5], L.Doria[8], P.Gumplinger[8], A.Hussein[9], Y.Igarashi[a], S.Kettell[b], L.Kurchaninov[8], L.Littenberg[b], C.Malbrunot[c,5], R.E.Mischke[8], T.Numao[8], D.Protopopescu[4], A.Sher[8], T.Sullivan[5], and D.Vavilov[8]

[1]Osaka University, Toyonaka, Osaka, 560-0043, Japan
[2]Instituto de Ciencias Nucleares, Universidad Nacional Autónoma de Mexico, México
[3]Virginia Tech., Blacksburg, VA 24061, USA
[4]University of Glasgow, Glasgow, UK
[5]University of British Columbia, Vancouver, B.C. V6T 1Z1, Canada
[6]Tsinghua University, Beijing, 100084, China
[7]Arizona State University, Tempe, AZ 85287, USA
[8]TRIUMF, 4004 Wesbrook Mall, Vancouver, B.C. V6T 2A3, Canada
[9]University of Northern British Columbia, Prince George, B.C. V2N 4Z9, Canada
[a]KEK, 1-1 Oho, Tsukuba-shi, Ibaraki, 305-0801, Japan
[b]Brookhaven National Laboratory, Upton, NY 11973-5000, USA
[c]Present address: CERN, Genéve 23 CH-1211, Switzerland

E-mail: s-ito@kuno-g.phys.sci.osaka-u.ac.jp

Abstract. The PIENU experiment at TRIUMF aims to measure the branching ratio of pion decays $R = \Gamma(\pi^+\to e^+\nu_e + \pi^+\to e^+\nu_e\gamma)/\Gamma(\pi^+\to\mu^+\nu_\mu + \pi^+\to\mu^+\nu_\mu\gamma)$ with precision <0.1%, providing a stringent test of the Standard Model hypothesis of electron-muon universality and a search for new physics.

1. Introduction

The branching ratio of charged pion decays $R = \Gamma(\pi^+\to e^+\nu_e + \pi^+\to e^+\nu_e\gamma)/\Gamma(\pi^+\to\mu^+\nu_\mu + \pi^+\to\mu^+\nu_\mu\gamma)$ is one of the most precisely calculated observables in the Standard Model (SM) involving quarks[1]. The most recent theoretical evaluation[2] gives

$$\begin{aligned} R_{SM} &= \frac{g_e^2}{g_\mu^2}\frac{m_e^2}{m_\mu^2}\frac{(m_\pi^2-m_e^2)^2}{(m_\pi^2-m_\mu^2)^2}(1+\delta)(1+\epsilon) \\ &= (1.2352\pm0.0001)\times10^{-4}. \end{aligned} \quad (1)$$

where g_e and g_μ are the coupling constants between the W boson and the electron or muon, m_e, m_μ, and m_π are the electron, muon, and pion masses, and the terms $(1+\delta)(1+\epsilon)$ come from radiative corrections; inner bremsstrahlung and emission and reabsorption of virtual photons result in $\delta = -(3\alpha/\pi)\ln(m_\mu/m_e)$ and $\epsilon = -0.92(\alpha/\pi)$. Precise measurement of R provides one of the most stringent tests of the hypothesis of electron-muon universality ($g_e = g_\mu$) in weak interactions. The current experimental values of the branching ratio are

$$R_{EXP1} = (1.2265\pm0.0034(stat)\pm0.0044(syst))\times10^{-4}(\text{TRIUMF},\ 1992)[3] \quad (2)$$

and

$$R_{EXP2} = (1.2346 \pm 0.0035(stat) \pm 0.0036(syst)) \times 10^{-4} (\text{PSI, } 1993)[4] \quad (3)$$

indicating that there is room for improvement by two orders of magnitude in precision.

Table 1 shows the current experimental results of electron-muon universality tests. The goal of the PIENU experiment at TRIUMF is to improve the accuracy of the branching ratio measurement by a factor of 5, to <0.1% resulting in 0.05% precision in the universality test. This precision also allows potential access to new physics up to the mass scale of 1000 TeV for helicity unsuppressed pseudoscalar interactions[1]. Examples of the new physics probed include R-parity violating SUSY[5], heavy neutrino mixing[6], excited gauge bosons, leptoquarks[7], compositeness, and the effects of charged Higgs bosons.

The PIENU experiment collected 6×10^6 $\pi^+\to e^+\nu_e$ events during run periods from 2009 to 2012 corresponding to more than 30 times higher statistics than in the previous TRIUMF experiment[3]. The initial analysis discussed here represents 5% of the statistics of the full data.

Table 1. Universality tests.

Decay Mode	g_μ/g_e
$\tau\to\mu/\tau\to e$	1.0018±0.0014[8]
$\pi\to\mu/\pi\to e$	1.0021±0.0016[3][4]
$K\to\mu/K\to e$	0.996±0.005[9]
$K\to\pi\mu/K\to\pi e$	1.002±0.002[10]
$W\to\mu/W\to e$	0.997±0.010[10]

2. The PIENU Experiment

2.1. Strategy

The decays $\pi^+\to e^+\nu_e$, and $\pi^+\to\mu^+\nu_\mu$ followed by $\mu^+\to e^+\nu_e\bar{\nu}_\mu$ decays (the $\pi^+\to\mu^+\to e^+$ decay chain) have different energy and time characteristics that can be precisely measured and used to extract the branching ratio. Figure 1 shows a schematic of pion decays and the measurement method. Positive pions stop in a plastic scintillator target and decay to muons or positrons. The muon in $\pi^+\to\mu^+\to e^+$ has kinetic energy $T_\mu = 4.1$ MeV and range in plastic scintillator of about 1 mm; the total energy of decay positrons has a continuous distribution from 0.5 to 52.8 MeV. The decay $\pi^+\to e^+\nu_e$ produces a mono-energetic positron at 69.8 MeV. In the PIENU experiment, the branching ratio is obtained from the ratio of the positron yields from $\pi^+\to e^+\nu_e$ decays and $\pi^+\to\mu^+\to e^+$ decays by taking advantage of these differences. Figure 2(a) shows the energy spectra of decay positrons in the calorimeter produced by a Monte Carlo (MC) simulation. Two energy regions, below and above the $\pi^+\to\mu^+\to e^+$ distribution shown as the dashed black line in Figure 2(a) are used to determine the time spectra of the decay positron. Figure 2(b) shows the time spectra in the low and high energy regions, respectively. These time spectra are distributed as

$$\pi^+\to e^+\nu_e : \varepsilon_{\pi\to e\nu}(t) = \frac{1}{\tau_\pi}\exp(-\frac{t}{\tau_\pi}) \quad (4)$$

$$\pi^+\to\mu^+\to e^+ : \varepsilon_{\pi\to\mu\to e}(t) = \frac{1}{\tau_\mu-\tau_\pi}\left\{\exp(-\frac{t}{\tau_\mu})-\exp(-\frac{t}{\tau_\pi})\right\} \quad (5)$$

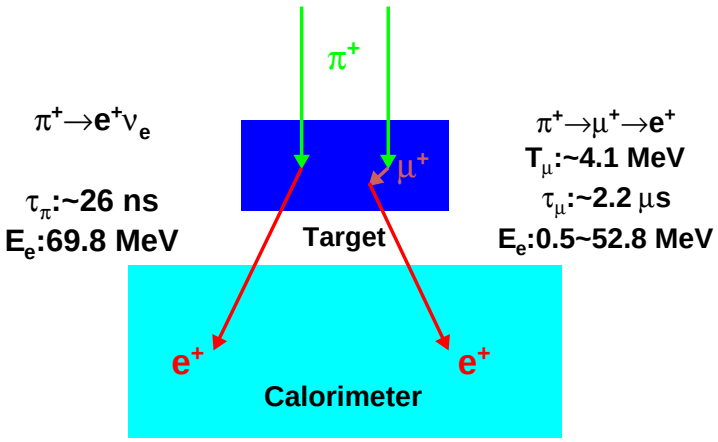

Figure 1. Schematic of the PIENU experiment technique (see text).

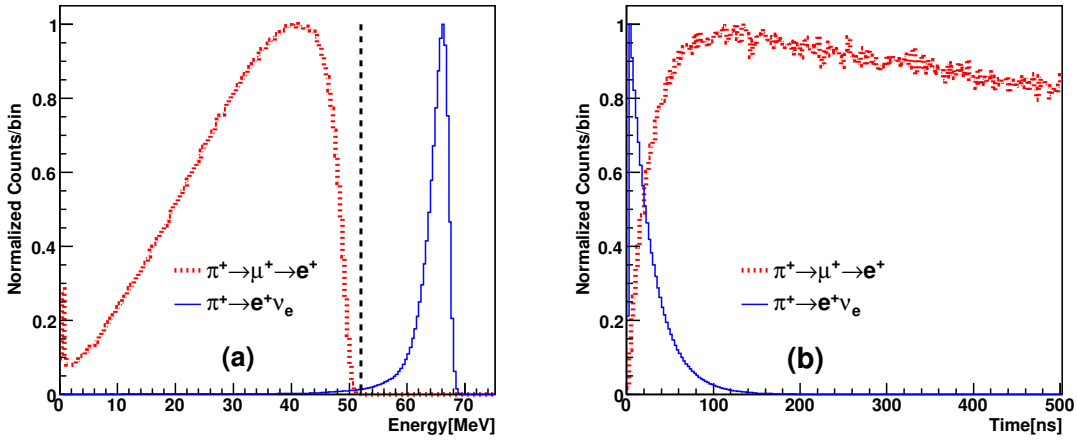

Figure 2. (a) Simulated energy spectra of decay positrons in the calorimeter. The horizontal axis is energy and the vertical axis is the amplitude normalized separately for the two modes. (b) Simulated decay positron time spectra. The horizontal axis is the decay time and the vertical axis is the amplitude normalized separately for the two modes.

where τ_π and τ_μ are the lifetimes of the pion and muon. The time spectra in the two regions are fitted to Eqs. (4) and (5) simultaneously in order to extract the "raw" branching ratio to which corrections are applied. The most important corrections resulting in systemmatic uncertainties include the $\pi^+ \to e^+ \nu_e$ low energy distribution in the calorimeter due to shower leakage and the difference of positron acceptances between $\pi^+ \to e^+ \nu_e$ and $\pi^+ \to \mu^+ \to e^+$ events. The raw branching ratio extraction and these systematic corrections will be discussed in Section 3.

2.2. Beam Line

The PIENU experiment was located at the TRIUMF M13 beam line. The TRIUMF cyclotron delivered a 500 MeV proton beam with an intensity of 120 μA to a 12 mm thick beryllium pion production target every 43 ns with a 4 ns wide pulse. In order to reduce the positron

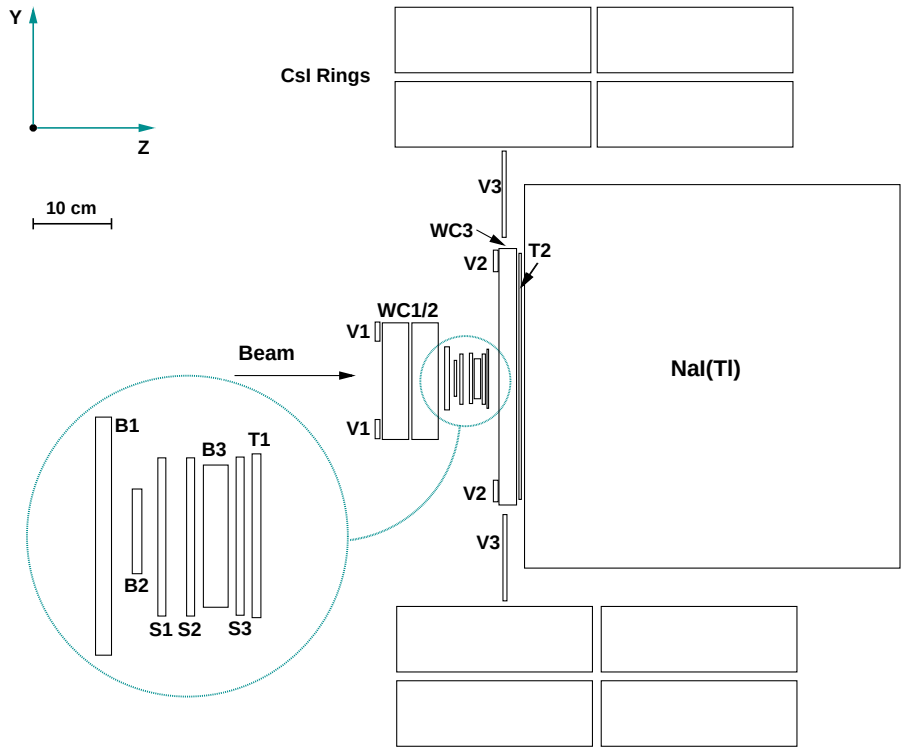

Figure 3. The schematic of the PIENU detector.

contamination in the beam, the M13 channel was modified[11]. A positive charged beam of momentum P=75±1 MeV/c was collected at 135^o and transported in vacuum to the PIENU detector. The pion beam rate was about 70 kHz and the beam was composed of 84% π^+, 14% μ^+, and 2% e^+.

2.3. The PIENU Detector

Figure 3 shows the schematic of the PIENU detector. Pion beam tracking was provided by two circular multiwire proportional chambers (WC1 and WC2) each with three planes oriented at 0° and ±120° at the exit of the beam line. Following WC2, the beam was degraded by two thin plastic scintillators B1 and B2 (beam counters) used for time and energy loss measurements in order to identify the beam pions. The beam counters were followed by two sets of single-sided 0.3-mm thick 61×61 mm^2 Si strip detectors (S1 and S2) with strips oriented along the X and Y axes. The pion beams stopped in the center of an 8 mm plastic scintillator target (B3) and decayed at rest.

In order to reconstruct the tracks and define the acceptance of decay positrons, another pair of X-Y Si strips (S3) and three layers of circular multiwire proportional chamber (WC3) were employed. Two thin plastic scintillators (telescope counters T1 and T2) were used to measure decay times and to define the on-line trigger. Triggered decay positrons entered a large single crystal NaI(Tl) calorimeter (48 cm diameter × 48 cm width). Two layers of 97 pure CsI pentagonal crystals of 25 cm in length surrounded the NaI(Tl) crystal for shower leakage detection. Three veto scintillators were installed to cover inactive material. V1 covered the front frame of WC1, V2 covered the frame of WC3, and V3 covered the front flange of the NaI(Tl) crystal. The solid angle acceptance was 20%, about 10 times larger than in the previous TRIUMF experiment[3].

2.4. The Trigger Logic

In the trigger logic, a coincidence of beam counters and B3 defined the pion signal, and a coincidence of positron signals in the telescope counters defined the decay positron signal. A coincidence of pion and decay positron signals within a time window of −300 ns to 540 ns with respect to the pion signal was the basis of the main trigger condition. Since $\pi^+ \to \mu^+ \to e^+$ decays happen much more often than $\pi^+ \to e^+ \nu_e$ decays, only 1/16 of these events were selected by the unbiased trigger (Prescale trigger). On the other hand, $\pi^+ \to e^+ \nu_e$ events were enhanced for the Early trigger and the HE (High Energy) trigger. The Early trigger selected the events in the early time window (4 ns to 40 ns) after pion decay and the HE trigger selected events with $E_e > 45$ MeV. The typical trigger rate was about 600 Hz, of which 240 Hz was for Prescale, 160 Hz for Early, 170 Hz for HE, and 20 Hz for the sum of calibration triggers. The waveforms from all scintillators, S1-3, NaI(Tl) and CsI crystals were digitized and time information from all sense wires of WC1-3 and signals used for the trigger logic were recorded.

3. Analysis -Raw Branching Ratio Extraction-

3.1. Event Selection

The charge and time information of each pulse were extracted from the waveforms. The charge was obtained by integrating the pulse for 40 ns for plastic scintillators, for 160 ns for S1-3 and CsI, and for 1 μs for the NaI. The waveforms in B1, T1, and B3 were fitted to the templates of each waveform for the best timing and particle identification purposes. B1 defined the pion timing ($t_{\rm B1}$) and T1 defined decay positron timing ($t_{\rm T1}$). $\pi^+ \to e^+ \nu_e$ decay has two pulses in B3, while $\pi^+ \to \mu^+ \to e^+$ decay has three pulses in B3 because of the additional decay muon.

The beam pions were selected by their energy loss in B1 and B2. The beam positrons and muons were negligible after the energy loss cut. The beam profile in WC1 and WC2 was used to remove particles which had unusual trajectories. Any events with extra hits in the beam counters and telescope counters in the time regions of -6.39 to 1.35 μs with respect to $t_{\rm B1}$ were removed. A radial acceptance cut in WC3 using tracks reconstructed with S3 and WC3 was used to reduce shower leakage from the NaI. This acceptance cut required that the radius at WC3 was < 60 mm.

Figure 4 shows examples of event selection cuts, the energy loss in B1 and the radius distribution of events at WC3. In the PIENU analysis, in order to avoid bias, the raw branching ratio was shifted by a hidden random value within 1% ("blinding"). Before unblinding the analysis, all systematic corrections and cuts are being studied and the stability of the results is being examined.

3.2. Time Spectra Fitting

Figure 5 is the spectrum of the NaI and CsI energies after event selection. It shows the $\pi^+ \to e^+ \nu_e$ peak and the continuous spectrum of $\pi^+ \to \mu^+ \to e^+$ decays. The raw branching ratio was extracted by performing a simultaneous fit of the time spectra using an energy threshold (E_{Cut}) at 52 MeV. Figure 6 shows the time spectra in the low energy region (a) and the high energy region (b). The events in the low energy region were triggered by the Prescale trigger and the Early trigger, while the HE trigger was used for the events in the high energy region.

In the low energy time spectrum, the components included were $\pi^+ \to \mu^+ \to e^+$ decays and muon ($\mu^+ \to e^+ \nu_e \overline{\nu}_\mu$) decays. $\pi^+ \to \mu^+ \to e^+$ decays are described by Eq. (5), and muon decays arising from pion-decay-in-flight (πDIF) and previous pion stops in B3 ("old-muons") are distributed as

$$\mu^+ \to e^+ \nu_e \overline{\nu}_\mu : \varepsilon(t)_{\mu \to e \nu_e \overline{\nu}_\mu} \;=\; \frac{1}{\tau_\mu} \exp(-\frac{t}{\tau_\mu}). \tag{6}$$

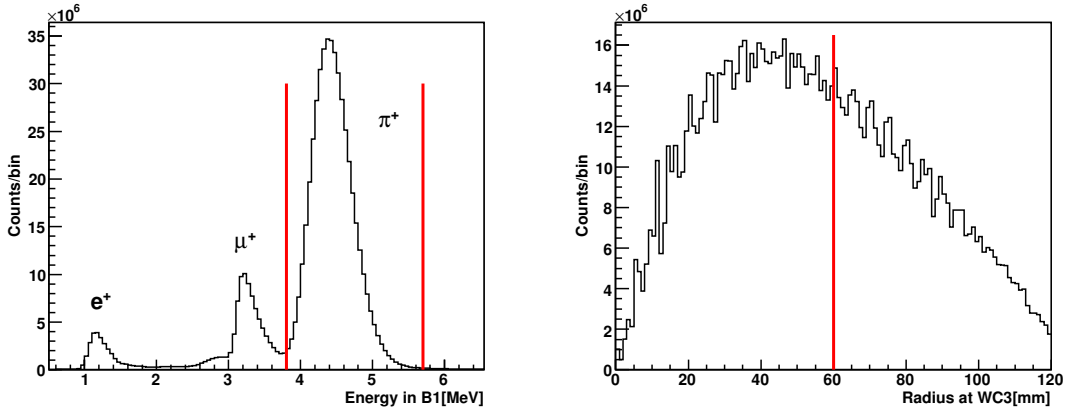

Figure 4. Event selection cuts. Left: Energy loss in B1. Right: Acceptance cut in WC3. Vertical red lines indicate cut values.

The $\pi^+ \to \mu^+ \to e^+$ and πDIF distributions begin at time $t = 0$. The solid red line, dashed dark blue line, and dashed pink line in Figure 6 (a) indicate $\pi^+ \to \mu^+ \to e^+$ decays, πDIF events, and previously arrived muons ("old-muons"). The distributions coming from multiple muon decays and the low energy tail of $\pi^+ \to e^+ \nu_e$ decays were estimated to contribute $< 0.01\%$ to the branching ratio, and were neglected in the time fit.

The main component in the high energy time spectrum was due to the $\pi^+ \to e^+ \nu_e$ decays distributed as Eq. (4). The major backgrounds were muon decays ($\pi^+ \to \mu^+ \to e^+$, πDIF, and old-muons) which were promoted to the high energy time spectrum by the energy resolutions of the NaI and CsI crystals, radiative muon decays in which the γ-ray increases the apparent positron energy, and pileup events in the calorimeter with a flat time distribution (e.g. due to neutrons coming from the production target). These components have the same time distribution in the low energy region. $\pi^+ \to \mu^+ \to e^+$, πDIF, and old-muon decays in the high energy region are shown as the solid blue line, the dashed dark blue line, and the dashed pink line in Figure 6(b) (colors on-line).

Another background in the high energy region came from radiative pion decays $\pi^+ \to \mu^+ \nu_\mu \gamma$ (branching ratio, 2×10^{-4}[12]) followed by $\mu^+ \to e^+ \nu_e \overline{\nu}_\mu$ decays. The time of the γ-ray is different from that of the decay positron. These contributions were estimated by MC simulation by using a waveform template for the NaI and CsI detectors. The amplitude of the $\pi^+ \to \mu^+ \nu_\mu \gamma$ component due to the E_{Cut} was 0.4% of the $\pi^+ \to e^+ \nu_e$ decays. The amplitude was fixed in the fitting function. This distribution ($\mathcal{G}$) is shown as the light blue line in Figure 6(b).

The distribution shown by the dashed violet line in the high energy region in Figure 6 (b) which arises from the $t < 0$ region and decreases in the $t > 0$ region is the pileup component of $\pi^+ \to \mu^+ \to e^+$ decays plus old-muon decays. The shape of this background was obtained by MC simulation using the pulse shapes of the NaI and CsI detectors. This function is represented by $\mathcal{F}_1$.

The pileup cut was based on the pulse shape in T1. If extra hits were observed in T1, the event was rejected. However, two events occurring within the double pulse resolution time of T1 were accepted. The shape of this distribution was the same as that for the pileup components of $\pi^+ \to \mu^+ \to e^+$ decays plus old-muon decays but with a short effective time constant ($\Delta T = 15$ ns). The effect of pileup coming within the double pulse reloluton time in T1 was estimated by artificially increasing the double pulse resolution time up to 150 ns. The amplitude of this component was estimated to be 4% of $\pi^+ \to e^+ \nu_e$ decays. This distribution is shown by the

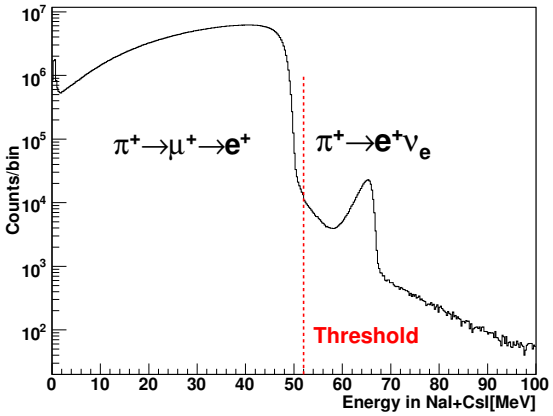

Figure 5. Combined energy spectrum of NaI plus CsI detectors. The vertical red line indicates the E_{Cut}=52 MeV.

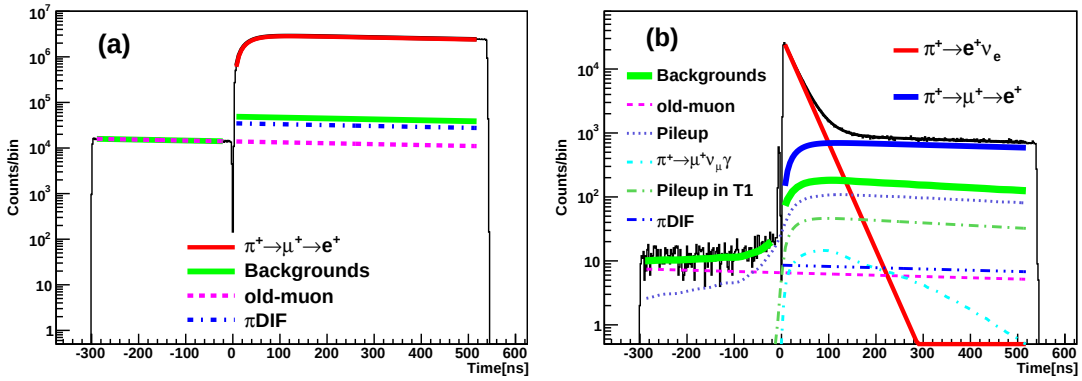

Figure 6. Time spectra in the low (a) and high (b) energy regions. Horizontal axes are decay times ($t_{T1} - t_{B1}$). The solid red lines in the low and high energy regions are $\pi^+ \to \mu^+ \to e^+$ and $\pi^+ \to e^+ \nu_e$, respectively. Other lines indicate background components and the solid green lines in both regions are the sums of the background components. See text for details.

dashed green line in Figure 6(b) and its function is represented by $\mathcal{F}_2$.

The following equations give the fitting functions in the low (PIMUE(t)) and high (PIENU(t)) energy regions as discussed above:

$$\text{PIMUE}(t) = \mathcal{H}(t)\left[a(1-r)\varepsilon_{\pi\to\mu\to e}(t) + b\varepsilon(t)_{\mu\to e\nu_e\overline{\nu}_\mu}\right] + c\varepsilon(t)_{\mu\to e\nu_e\overline{\nu}_\mu} \quad (7)$$

$$\text{PIENU}(t) = \mathcal{H}(t)\left[a\{(R + C_{\mu DIF})\varepsilon(t)_{\pi\to e\nu} + d\mathcal{G}(t) + r\varepsilon_{\pi\to\mu\to e}(t)\} + b'\varepsilon(t)_{\mu\to e\nu_e\overline{\nu}_\mu}\right] + c'\varepsilon(t)_{\mu\to e\nu_e\overline{\nu}_\mu} + e\mathcal{F}_1 + f\mathcal{F}_2 \quad (8)$$

where R is the raw branching ratio, $\mathcal{H}(t)$ is the Heaviside step function ($\mathcal{H}(t>0)=1$, $\mathcal{H}(t<0)=0$), $\varepsilon(t)_{\pi\to e\nu}$, $\varepsilon_{\pi\to\mu\to e}(t)$, and $\varepsilon(t)_{\mu\to e\nu_e\overline{\nu}_\mu}$ are the same functions as in Eq. (4),(5) and (6), and $t = t' - t_0$ where t' is the measured time and t_0 is the pion stop time which was determined by prompt events and is fixed in the fit. The choice of t_0 doesn't affect the branching ratio. In Eqs.

(7) and (8), the parameter a represents the number of $\pi^+ \to \mu^+ \to e^+$ decays, and ar indicates the number of $\pi^+ \to \mu^+ \to e^+$ decays in the high energy region. The other parameters b, b', c, c', d, e, and f are the amplitudes of each function. The free parameters are R, a, r, b, c, c' and e. Parameters d, e, f and $C_{\mu DIF}$ are fixed to the estimated amplitudes. However, the correlation between πDIF decays and old-muon decays or $\mathcal{F}_1$ was significant. Therefore, parameter b' is scaled to the amplitude of πDIF in the low energy region; namely, $b' = rb$. The parameter $C_{\mu DIF}$ was the corrected amplitude for muon-decay-in-flight (μDIF) events, which will be discussed in the next section. The fitting range was from -290 to 520 ns omitting the prompt region of -20 to 5 ns.

The raw branching ratio remains blinded at the time of writing. The statistical uncertainty of the raw branching ratio was 0.2%.

4. Analysis -Systematic Sources-

4.1. Tail Correction

The largest correction to the branching ratio came from knowledge of the low energy $\pi^+ \to e^+ \nu_e$ tail events below E_{Cut} which were buried under $\pi^+ \to \mu^+ \to e^+$ distribution. In order to evaluate this correction it was necessary to suppress the dominant $\pi^+ \to \mu^+ \to e^+$ component. This was done using four suppression factors. First, by exploiting the short pion lifetime compared to muon lifetime, the early time region $5 - 35$ ns after the pion stop enriched $\pi^+ \to e^+ \nu_e$ decays relative to $\pi^+ \to \mu^+ \to e^+$ events by a factor of 100. The second factor was obtained using the energy loss and pulse shape information in B3. For $\pi^+ \to e^+ \nu_e$ decays, the energy loss in B3 was the sum of the kinetic energy of the stopping pion plus a small contribution from the exiting decay positron. On the other hand, $\pi^+ \to \mu^+ \to e^+$ decays had an additional 4.1 MeV deposited from the kinetic energy of the decay muon which stopped in B3. As shown in Figure 7(a), there are two peaks in the spectrum of total energy deposited by beam pions in B1, B2, S1, S2, and B3. The cut region indicated by two vertical red lines in Figure 7(a) provided a factor of > 100 suppression.

The third $\pi^+ \to \mu^+ \to e^+$ suppression factor employed beam pion tracking by S1 and S2 in order to reject πDIF events before B3. πDIF events may result in a mismatch of the particle trajectory as determined by WC1 and WC2 compared to that obtained using S1 and S2, as illustrated in Figure 7(b). These events left energy in B3 similar to $\pi^+ \to e^+ \nu_e$ events but had a larger mismatched ("kink") angle than decay-at-rest events. The fourth factor was found using the energy loss in S3. About 30% of muons from πDIF events traversed B3 and deposited larger energy than the decay positron in S3. The fifth factor was based on the pulse shape fitting in B3. Multiplying the five suppression factors gave a total suppression of 10^5.

Figure 8 shows the suppressed energy spectra. In order to evaluate the correction for the $\pi^+ \to e^+ \nu_e$ low energy tail, the remaining $\pi^+ \to \mu^+ \to e^+$ events of the suppressed spectrum were subtracted and the $\pi^+ \to e^+ \nu_e$ tail was obtained. Additionaly, since the total energy cut removed $\pi^+ \to e^+ \nu_e$ events with Bhabha scattering and larger energy loss in B3, MC simulation was used to take account of those events. These procedures were based on the method of the previous TRIUMF experiment[3]. The tail fraction found was 3% which provides a lower bound on this correction.

In order to determine an upper bound of the $\pi^+ \to e^+ \nu_e$ low energy tail empirically, special data sets were taken using a 70 MeV/c positron beam. The left diagram in Figure 9 shows a schematic of the lineshape measurement. The crystal calorimeter was rotated to obtain different angles of entry. The right plot in the figure is the energy spectrum at 0°. It shows the peak of the beam positrons as well as three lower energy bumps due to photoabsorption followed by neutron escape from the NaI crystal[14]. The $\pi^+ \to e^+ \nu_e$ lineshape distribution using these beam measuements as input was then obtained by simulation. The fraction of the events below E_{Cut} was estimated to be 3% in agreement with the lower bound discussed above. The tail fraction

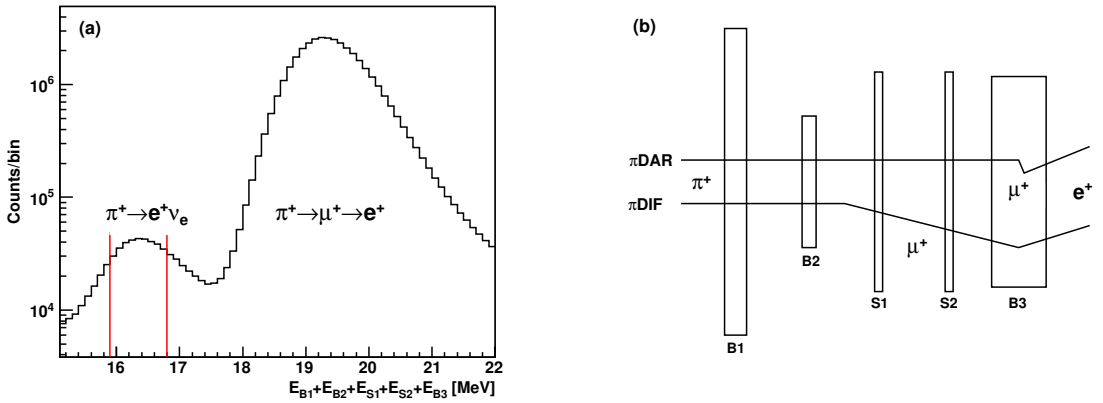

Figure 7. (a) Total energy deposited in B1, B2, S1, S2, and B3. (b) Schematic of π-decay-at-rest (πDAR, upper trajectory) and πDIF (lower trajectory) events.

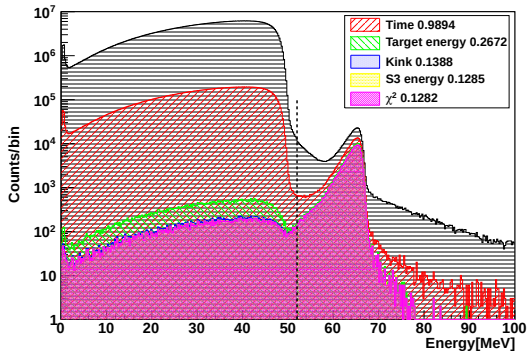

Figure 8. Summed energy spectrum of NaI and CsI after each suppression cut. The black histogram (top line) is before suppression and the pink histogram (filled) is after all suppression cuts. The legend box shows the low energy fraction, which represents the integral of events below E_{Cut}(=52 MeV) divided by the integral of the full energy spectrum.

obtained by this method was used as an upper bound.

Assuming a normal distribution for the probability distribution function, the combined tail fraction was estimated to be 3%.

4.2. Acceptance Correction

Energy dependent effects altered the relative acceptance of $\pi^+\to e^+\nu_e$ and $\pi^+\to\mu^+\to e^+$ decays. The acceptance correction relied on MC calculations including multiple Coulomb scattering, Bhabha scattering, positron annihilation-in-flight, and trigger losses. The ratio of acceptance of $\pi^+\to e^+\nu_e$ and $\pi^+\to\mu^+\to e^+$ decays was estimated to be 0.9994 for the radius cut < 60 mm at WC3. The uncertainties of the detector geometry and the pion beam stopping position were included in the error.

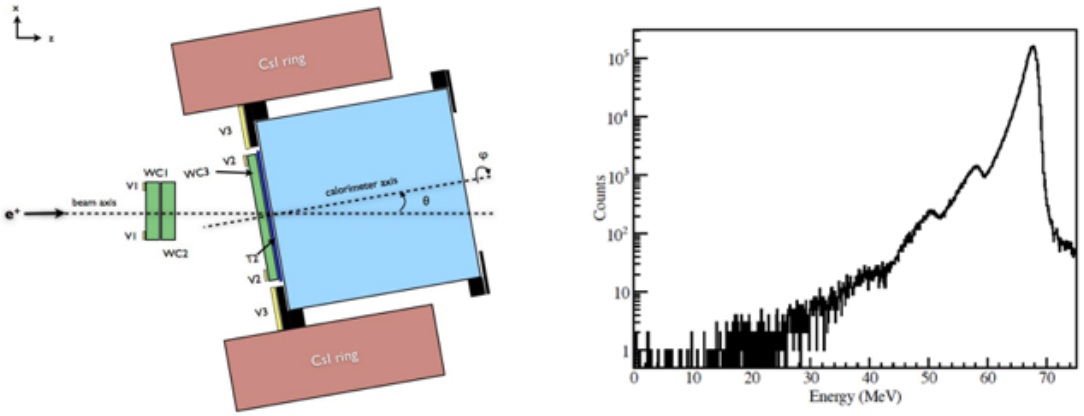

Figure 9. Left: Schematic of the calorimeter lineshape measurement.[13] Right: Energy spectrum in NaI and CsI at 0°[14].

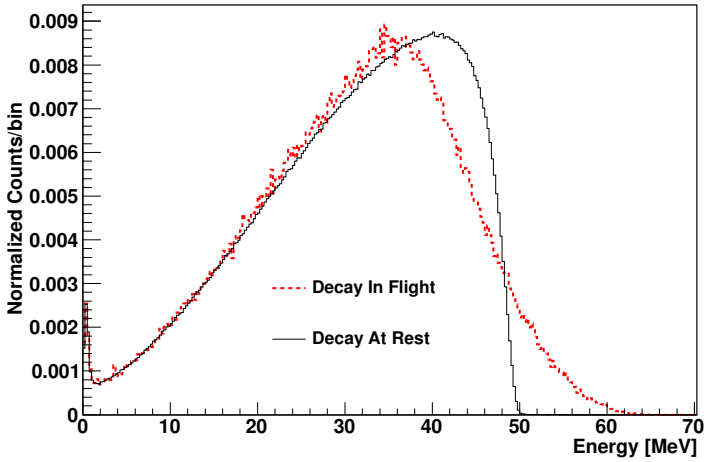

Figure 10. $\pi^+ \to \mu^+ \to e^+$ energy spectra. Red (dashed line): Simulated μDIF events. Black (solid line): Decay-at-rest events.

4.3. Uncertainty of the μDIF Contribution

For the decays-in-flight of muons from $\pi^+ \to \mu^+ \nu_\mu$ in B3, Lorentz boosting raises the positron energy. Figure 10 shows the energy spectra of μDIF and μ-decay-at-rest events determined by MC. Since μDIF had the same time distribution as $\pi^+ \to e^+ \nu_e$ decays, μDIF events inflated the apparent number of $\pi^+ \to e^+ \nu_e$ decays. The contribution of μDIF events $C_{\mu DIF}$ was estimated by MC study and scaled to the number of $\pi^+ \to \mu^+ \to e^+$ decays (parameter A) in Eq.7. The correction value $C_{\mu DIF}$ was found to be 0.2% of $\pi^+ \to e^+ \nu_e$, resulting in an uncertainty on the branching ratio $< 0.01\%$.

4.4. Other Corrections

The timing of the decay positron was based on the signal from energy loss in T1. Possible energy dependence with the pion stop time t_0 was studied using decay positrons from muons stopped

at the center of B3. It was also found that the effect of the uncertainty of the muon lifetime[15] on the branching ratio was $< 0.01\%$ while the pion lifetime[15] uncertainty contributed 0.01%.

5. Result and Conclusion

At present, the result for the $\pi^+ \to e^+ \nu_e$ branching ratio for the initial data set analyzed remains blinded. The expected statistical and systematic uncertainties with the current partial data set are both about 0.2%. The full data set is currently under analysis and corresponds to 20 times higher statistics. It is anticipated that the systematic uncertainties will also be substantially improved.

References

[1] Rare Pion and Kaon Decays, D. Bryman, W. Marciano, R. Tschirhart, T. Yamanaka, Ann. Rev. Nucl. Part. Sci. 61, 331 (2011).
[2] V. Cirigliano and I. Rosell,*JHEP* **0710**, 005 (2007).
[3] D.I. Britton *et al.*, *Phys. Rev. Lett.* **68**, 3000 (1992). and D.I. Britton *et al.*, *Phys. Rev.* D**49**, 28 (1994).
[4] G. Czapek *et al.*, *Phys. Rev. Lett.* **70**, 17 (1993).
[5] M.J. Ramsey-Musolf, S. Su and S. Tulin, *Phys. Rev.* D**76**, 095017 (2007).
[6] H. Lacker and A. Menzel, *JHEP* **07**, 006 (2010).
[7] S.Davidson, D. Bailey and B. Campbell, *Z. Phys.* C**61**, 613 (1994).
[8] Alberto Lusiani. Measurements of $|V_{us}|$ and Search for Violation of Lepton Universality and CPT in Tau Decay at BABAR. *PoS*, ICHEP2010:251, 2010. arXiv:1012.3734.
[9] C. Lazzeroni *et al.* Test of Lepton Flavour Universality in $K^+ \to l\nu$ Decays, 2011. arXiv:1101.4805.
[10] A. Pich. Tau Physics: Theory Overview. *Nucl. Phys. Proc. Suppl.*, 181-182:300-305 (2008).
[11] A. Aguilar-Arevalo *et al.*, *Nucl. Instrum. Method* A**609**, (2009) 102.
[12] G. Bressi, *et al.*, *Nucl. Phys.* **B513** (1998) 555.
[13] C.Malbrunot. *Study of* $\pi^+ \to e^+ \nu_e$ *decay.* PhD thesis, University of British Columbia. (2012).
[14] A. Aguilar-Arevalo, *et al.*, Study of a Large NaI(Tl) Crystal, *Nucl. Instrum. Meth.* A**621** (2010) 188191.
[15] K.A. Olive *et al.* (Particle Data Group), *Chin. Phys.* **C38** 090001 (2014).